Effects of Alkyl Amide Solvents on the Dispersion of Single-Wall Carbon Nanotubes

Brian J. Landi,[†] Herbert J. Ruf,[†] James J. Worman,[‡] and Ryne P. Raffaelle*[,†]

NanoPower Research Laboratories (NPRL) and Department of Chemistry, Rochester Institute of Technology, Rochester, New York, 14623

Received: June 8, 2004; In Final Form: August 26, 2004

Stable dispersions of both as-produced (raw soot) and purified laser-generated single-wall carbon nanotubes (SWNTs) have been demonstrated with several alkyl amide solvents. Optical absorption analysis over a range of concentrations has been utilized to estimate the dispersion limits for as-produced SWNTs in *N*,*N*-dimethylformamide (DMF), *N*,*N*-dimethylacetamide (DMA), *N*,*N*-diethylacetamide (DEA), and *N*,*N*-dimethylpropanamide (DMP). In addition, extinction coefficients have been calculated using Beer's law for each solvent at energies of 1.27 and 1.77 eV, corresponding to the electronic transitions of semiconducting and metallic SWNTs, respectively. The results imply that high polarizability and optimal geometries (appropriate bond lengths and bond angles) may account for the favorable interaction between SWNTs and the alkyl amide solvents. The successful dispersion of purified SWNTs in DMA has enabled extinction coefficients of 43.4 and 39.0 mL·mg^{-1}·cm^{-1} to be calculated at the selected energies, respectively. The magnitude of the dispersion limit and extinction coefficient values has been shown to be strongly dependent on the SWNT sample purity. These findings offer the potential for solution-phase analysis of SWNTs directed at purity assessment and electrophoretic separations in a simple organic solvent.

Introduction

Single-wall carbon nanotubes (SWNTs) have shown tremendous potential in a number of applications on the basis of their unique electronic and structural properties.[1] The opportunity to exploit these properties depends on the successful characterization and manipulation of desired materials. In some cases, the necessity to utilize solution-phase techniques is hindered by the inability to form stable SWNT dispersions. Many groups have resorted to functionalization strategies,[2,3] including the use of polymers,[4,5] surfactants,[6,7] and amines, to assist in dispersing SWNTs.[8−10] However, these techniques may disrupt the SWNT structure, may alter the electronic properties, or may be problematic for subsequent removal.[11] Therefore, the dispersion of high aspect ratio, raw and purified SWNTs in a suitable solvent is necessary to enable more accurate solution-phase analyses.

The most promising attempts at forming stable SWNT dispersions have been with organic amide solvents such as *N*,*N*-dimethylformamide (DMF) and *N*-methylpyrrolidone (NMP),[11,12] and with 1,2-dichlorobenzene for both HiPco and laser-generated SWNTs.[13] Calculation of the extinction coefficient at 2.48 eV (500 nm) for as-produced HiPco SWNTs in 1,2-dichlorobenzene was reported to be 28.6 mL·mg^{-1}·cm^{-1}.[13] This is higher than the recently reported value of 9.7 mL·mg^{-1}·cm^{-1} for arc-discharge-functionalized SWNTs in CS_2 at the same energy.[14] These results imply that variations exist for the extinction properties of SWNT materials, potentially occurring from differences in diameter distributions, purity, and/or solvent effects. Dispersion of SWNTs in the organic amide solvents has been attributed to the availability of a free electron pair and high solvatochromic parameter, π^*, although these characteristics are not sufficient, since they are also present in dimethyl sulfoxide (DMSO), which is inefficient at dispersing SWNTs.[11] Further work aimed at investigating the SWNT−solvent interaction may lead to improved dispersion limits and aid in the understanding of the extinction properties of SWNTs.

In this paper, we investigate the dispersion properties of both as-produced (raw soot) and purified laser-generated SWNTs with several alkyl amide solvents, namely, *N*,*N*-dimethylacetamide (DMA), *N*,*N*-dimethylpropanamide (DMP), and *N*,*N*-diethylacetamide (DEA). An improvement in the dispersion limit was observed for each of these in comparison with DMF and NMP. A mechanism is proposed to explain the interaction between the alkyl amide solvents and SWNTs on the basis of steric and electronic properties. These results demonstrate the ability to achieve well-resolved optical absorption spectra for SWNT characterization, with corresponding higher extinction coefficients for purified materials. Additionally, the potential exists for future improvements in applications such as electrophoretic separations, scattering studies, and organic reaction chemistry using SWNT−DMA dispersions.

Experimental Section

SWNT Synthesis, Characterization, and Purification. SWNTs were synthesized using the pulse laser vaporization technique, employing an Alexandrite laser (755 nm).[15] The laser pulse was rastered using GSI Lumonics mirrors over the surface of a graphite (1−2 μm) target doped with 2% w/w Ni (sub-μm) and 2% w/w Co (<2 μm), at an average power density of 100 W/cm^2. The reaction furnace temperature was held at 1150 °C, with a chamber pressure of 700 Torr under 100 sccm of flowing $Ar_{(g)}$. The raw SWNT soot was collected from the condensed region on the quartz tube at the rear of the furnace. Synthesis of a representative nanostructured carbon (NC) component in the raw soot was performed by laser vaporization at the described conditions for an undoped graphite target. The

* To whom correspondence should be addressed. E-mail: rprsps@rit.edu.
† NPRL.
‡ Department of Chemistry.

10.1021/jp047521j CCC: $27.50
Published on Web 10/12/2004

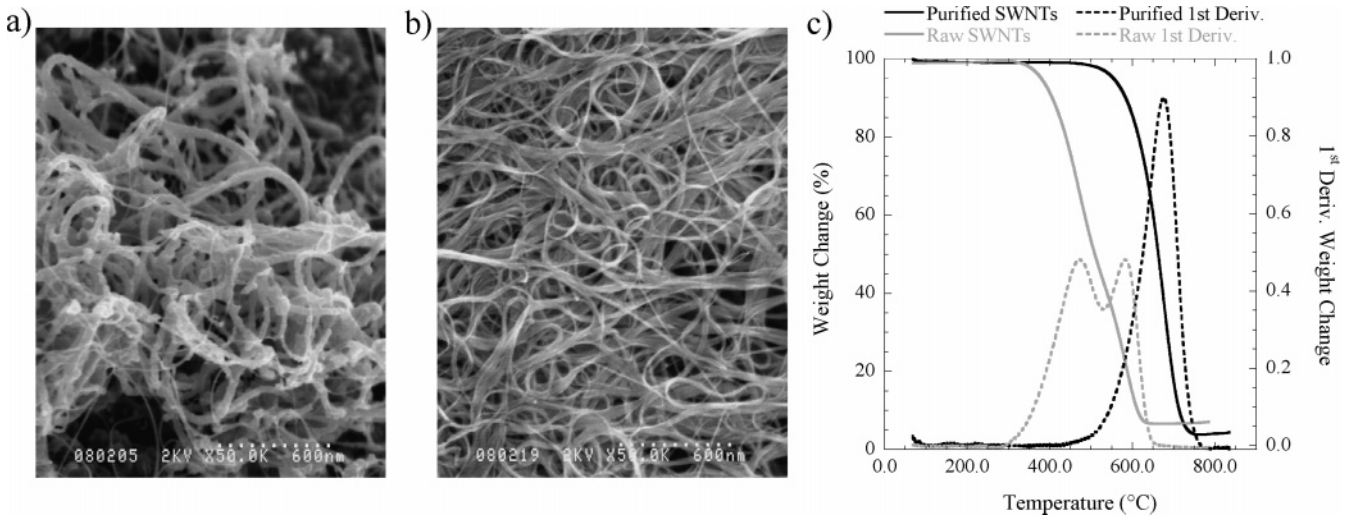

Figure 1. Representative SEM images of laser-generated (a) raw SWNT soot and (b) purified, >95% w/w SWNTs. The TGA overlay in (c) shows the thermal decomposition profile of (a) and (b) in air at a ramp rate of 5 °C/min.

NC material was devoid of SWNTs detectable by SEM, Raman, or optical absorption spectroscopies.

Analysis of SWNTs was performed by scanning electron microscopy (SEM), Raman spectroscopy, and thermogravimetric analysis (TGA). SEM was conducted using a Hitachi S-900, with samples applied directly to the brass stub using silver paint. The instrument was operated at an accelerating voltage of 2 kV, and magnifications ranged from 5000× to 250000×. Raman spectroscopy was performed at room temperature using a JY-Horiba Labram spectrophotometer with excitation energies of 1.96 and 2.54 eV. These energies have been shown to probe the metallic and semiconducting laser-generated SWNTs, respectively, over the range of diameters used in this study.[16] Sample spectra were obtained from 50 to 2800 cm^{-1} using an incident beam attenuation filter to eliminate localized heating and subsequent sample decomposition. TGA was conducted using a TA Instruments 2950. Samples were placed in the platinum pan balance in quantities of ~1 mg and ramped at 5 °C/min from room temperature up to 950 °C under air at a gas flow rate of 60 sccm and $N_{2(g)}$ balance purge at a gas flow rate of 40 sccm.

Purification of raw SWNT soot was performed using a modification of a previously reported procedure.[17] Approximately 50 mg of raw SWNT soot was brought to reflux at 125 °C in 3 M nitric acid for 16 h, and then filtered over a 1 μm PTFE membrane filter with copious amounts of water. The filter paper was rinsed consecutively with acetone, ethanol, 2.5 M NaOH, and H_2O until the filtrate became colorless after each step. The membrane filter was dried at 70 °C in vacuo to release the resulting SWNT paper from the filter paper. The SWNT paper was thermally oxidized in air at 550 °C for 1 min in a Thermolyne 1300 furnace. Finally, a 6 M hydrochloric acid wash for 60 min using magnetic stirring, with similar filtering steps and thermal oxidation at 550 °C for 20 min, completed the purification. SEM and TGA analyses were conducted during the purification process to ensure that the quality of the purification was at least 95% w/w SWNTs. In some cases, we have employed a postpurification annealing step at 1100 °C under flowing $Ar_{(g)}$, which is expected to remove structural defects and surface functionalization.[18]

SWNT−Solvent Dispersion Preparation. Stable dispersions of SWNTs in the evaluated solvents were achieved using a three-step process. Initially, stock solutions of 0.100 mg of SWNTs/mL of solvent were prepared and ultrasonicated (38.5−40.5 kHz) for 30 min at 40 °C. Serial dilutions with pure solvent were made to achieve the desired concentrations of 12.5, 6.25, 3.13, 1.56, 0.781, and 0.391 μg/mL. The ultrasonication step was performed prior to transferring each aliquot to the subsequent dilution. Next, each concentration was centrifuged at 5000 rpm for 10 min to remove any nondispersed material. The supernatant was decanted and analyzed using optical absorption spectroscopy.

Optical Absorption Spectroscopy. UV−vis−near-IR spectra were obtained using a Perkin-Elmer Lambda 900 spectrophotometer. Sample handling for dispersion solutions involved the use of 1 cm quartz cuvettes, while dry SWNT samples were air sprayed from a 0.1 mg/mL acetone solution onto 1 $in.^2$ quartz slides. The instrument scanned over a wavelength range of 300−1600 nm at a data interval of 1 nm. In the near-IR range, the instrument scan speed was 375 nm/min, with an integration time of 0.16 s, a 1.0 nm slit, and the gain set at 1. For the UV−vis region, the scan speed was 375 nm/min, with an integration time of 0.12 s, a 4.0 nm slit, and the gain set at 1.

It is well established that the diameter and electronic type of SWNTs are responsible for the unique set of transitions present in optical absorption spectroscopy.[16] The characteristic position of the absorption peaks corresponds to abrupt changes in the electronic density of states, or Van Hove singularities. The *i*th pair of discrete electronic transition energies corresponding to these singularities is approximated by the following:

$$^{S,M}E_{ii} = 2na_{c-c}\gamma_0/d_{SWNT}$$

where n is an integer, having values of 1, 2, 4, 5, or 7 for semiconducting (S) SWNTs and $n = 3$ or 6 for metallic (M) SWNTs in the spectral range of interest,[19] a_{c-c} is the carbon−carbon bond distance with a value of 0.142 nm, and d_{SWNT} is the SWNT diameter.[20,21] The carbon−carbon overlap integral, γ_0, for SWNTs has been reported to range from 2.45 to 3.0 eV.[22] The electronic transitions probed in this optical absorption analysis are $^{S}E_{22}$, $^{M}E_{11}$, $^{S}E_{33}$, $^{S}E_{44}$, and $^{M}E_{22}$, due to the absorption windows of the alkyl amide solvents.

Results and Discussion

Initially, characterization of the raw and purified SWNT materials was performed by SEM, TGA, and Raman spectroscopy. Shown in Figure 1a is a representative SEM image of

raw SWNT soot, with the distinguishing characteristics of amorphous carbon and metal catalyst impurities surrounding the SWNT bundles. Figure 1b shows an SEM image of the sample after the purification process, evident by the removal of the synthesis impurities. The TGA thermogram (see Figure 1c) indicates two prominent decomposition temperatures for the raw SWNT soot at 450 and 553 °C, with a metal oxide residue of 7.5% w/w. These decomposition temperature values are determined from the peak maxima of the first-derivative plots. The TGA data for the purified SWNTs show a single decomposition temperature at 677 °C with a metal oxide residue of 3.7% w/w. On the basis of these data and an analysis using optical absorption spectroscopy,[23] we estimate the raw soot to be ~30% w/w SWNTs and the purified SWNTs to be of a purity that is at least 95% w/w. Raman spectroscopy of the laser-generated SWNTs has shown the presence of both metallic and semiconducting SWNTs, each within a diameter range of 1.2−1.4 nm, on the basis of peak assignments of the radial breathing mode with the previously established relationship between the Raman shift and SWNT diameter (see Figure S1 in the Supporting Information).[24,25]

The ability to produce SWNT dispersions was first evaluated using a single batch of raw SWNT soot with the following alkyl amide solvents: NMP, DMF, DMA, DEA, and DMP. The stability of these dispersions was assessed after ultrasonication, centrifugation, and decantation steps. Optical absorption spectra were obtained for each prepared dispersion concentration to establish the dispersion limit using Beer's law plots.[26] This enabled both qualitative analysis of the dispersion limit for each solvent based on the presence of sediment after centrifugation and quantitative analysis using the absorbance measurements for each prepared dispersion concentration. In contrast to the previous report, NMP was inefficient at dispersing our raw SWNT soot after these processing steps; therefore, our initial comparison will only include the latter four amide solvents.[11] Shown in Figure 2a is a picture of the SWNT−solvent dispersions used during analysis, at a prepared concentration of 6.25 μg/mL. The corresponding optical absorption overlay for these SWNT−solvent dispersions is represented in Figure 2b. The variation in absorbance intensity can be attributed to each solvent's ability to disperse the raw SWNT soot. The largest absorbance and most well resolved spectrum were exhibited by the SWNT−DMA dispersion. The peaks corresponding to the electronic transitions for semiconducting ($^{S}E_{22}$, $^{S}E_{33}$, and $^{S}E_{44}$) and metallic ($^{M}E_{11}$) SWNTs are highlighted by the gray bands.[19] For this diameter distribution, the peak maxima for $^{S}E_{22}$ and $^{M}E_{11}$ occur at 1.27 and 1.77 eV, respectively. These selected energies were used to generate dispersion limit curves from each SWNT−solvent dispersion series.

The Beer's law plot in Figure 3a shows the absorbance measurements at 1.27 eV for SWNT−solvent dispersions over the concentration range examined. The dispersion limit can be estimated from the plot by generating a smooth curve fit (Kaleidagraph) and observing the point at which the data deviate from a linear trendline. The extent of the "knee" in the inflection point can be attributed to density variation between solvents, with DMF having the highest density (0.944 g/mL) and DEA having the lowest (0.925 g/mL). Therefore, since DMF has the smallest inflection, a linear trendline was generated from the four lowest concentrations (dashed line) to better illustrate its dispersion limit. Additionally, it is observed that the absorbance values continue to increase after the inflection point, resulting from the non-SWNT carbonaceous materials present in raw soot

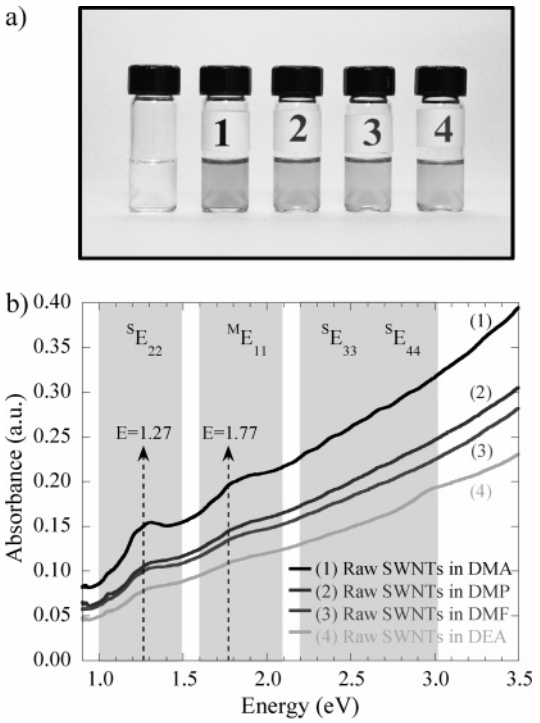

Figure 2. (a) Picture of the prepared 6.25 μg/mL SWNT−solvent dispersions used to generate the optical absorption data shown in (b). The colorless sample vial on the left is pure DMA, and the dispersions are (1) raw SWNTs in DMA, (2) raw SWNTs in DMP, (3) raw SWNTs in DMF, and (4) raw SWNTs in DEA. The gray bands in (b) depict the energy transition range for the current SWNT diameter distribution. The arrows designate the absorption maxima at 1.27 and 1.77 eV, corresponding to the second semiconducting and first metallic electronic transitions, respectively.

that is dispersed in these solvents. The results for the estimated dispersion limits of raw SWNT soot in each solvent are summarized in Table 1, but the general trend is as follows: DMA > DMP > DEA > DMF. The same trend was observed for absorbance measurements at 1.77 eV (Figure 3b), indicating that the dispersions are not type sensitive, but include both metallic and semiconducting SWNTs. The dispersion limit values are listed as the last data point, which was consistent with a linear trendline at $R^2 = 0.999$. In fact, the dispersion limit for DMA was a factor of 4 higher than that for DMF (i.e., 6.25 μg/mL compared to 1.56 μg/mL), an improvement over previous reports using DMF.[11,12] The dispersion limit curves from the Beer's law plot were corroborated by the presence of sediment after centrifugation for the concentrations which deviated from the linear trendline. SEM analysis of the sediment showed a morphology which was indistinguishable from the raw SWNT soot, evident by the presence of SWNTs, amorphous carbon, and metal catalyst impurities. The stability of the SWNT−alkyl amide solvent dispersions was observed to range from 12 to 24 h for concentrations near the dispersion limit, but on the order of days to a week for concentrations in the linear region of the Beer's law plot. The highest stability was observed for DMA, in good agreement with the dispersion limit trend.

Previous work using 1,2-dichlorobenzene (DCB) gives a higher dispersion limit of 95 μg/mL for raw HiPco, using a filtration method for estimating the dispersion limit.[13] A comparison of the use of DCB and DMA to disperse raw SWNT soot with the method used in our current study and the previously reported filtration methods in ref 13 has been performed. The same SWNT concentration series used above

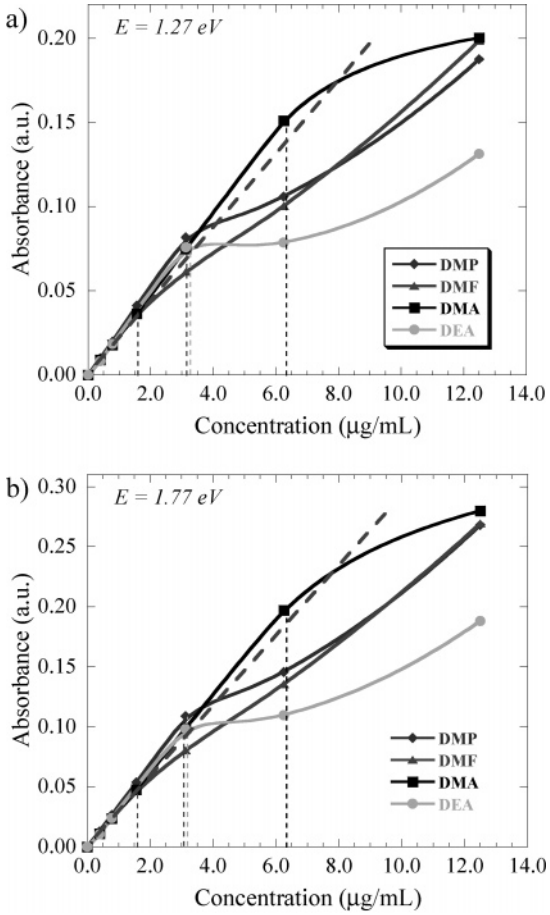

Figure 3. Beer's law plots for each prepared SWNT−solvent dispersion at (a) 1.27 eV and (b) 1.77 eV. The dispersion limit is estimated from the smooth curve fit at the last data point before the inflection, and is designated by the vertical dashed lines. The linear trendline (---) generated using the four lowest concentrations for the DMF dispersion series is provided to illustrate its dispersion limit. The experimental error is within the limits of the data points.

TABLE 1: Experimental Results for Dispersion Limit (D_L) Estimations and Extinction Coefficients of Raw SWNTs in Alkyl Amide Solvents, Including the Reported Dielectric Constants

solvent	D_L(raw SWNTs) (μg/mL)	$\epsilon_{1.27eV}$(raw SWNTs) (mL·mg^{-1}·cm^{-1})	$\epsilon_{1.77eV}$(raw SWNTs) (mL·mg^{-1}·cm^{-1})	dielectric constant[29]
DMF	1.56	23.4	30.0	37.06
DMA	6.25	23.8	31.2	38.30
DEA	3.13	24.2	31.3	31.33
DMP	3.13	26.1	34.7	33.08

was prepared for DCB and DMA through ultrasonication at 40 °C. No visual aggregates were observed in either solvent's solution for the 6.25 μg/mL prepared concentration. However, the presence of nondispersed particles was observed in both solvents for the 12.5 μg/mL prepared concentration. Unfortunately, due to the higher density of DCB (1.306 g/mL) compared to DMA (0.937 g/mL), the centrifugation technique was unsuccessful at removing the nondispersed particles in DCB. In addition, filtration in the presence of glass wool was seen to introduce variability in the absorption spectra of the resulting dispersions, possibly arising from the glass wool packing density and SWNT interactions during elution. Shown in Figure 4 is an overlay of the optical absorption spectra for the stable DCB and DMA dispersions at 6.25 μg/mL. The differences in absorbance values can be attributed to solvent effects, most

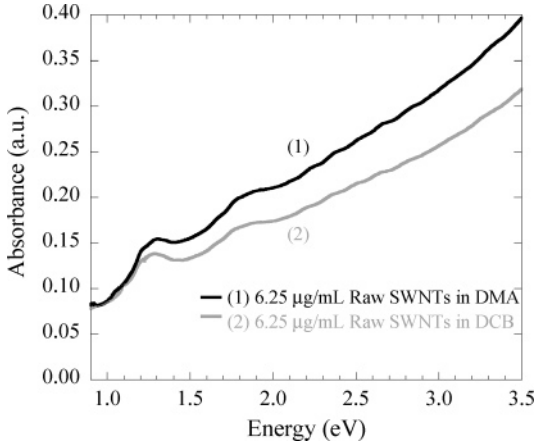

Figure 4. Optical absorption spectra for stable SWNT dispersions at a prepared concentration of 6.25 μg/mL for (1) DMA (black) and (2) DCB (gray).

notably the index of refraction for the individual solvents ($\eta^{20}_{DCB} = 1.551$ and $\eta^{20}_{DMA} = 1.438$).[27] Also, a blue shift of 22 meV was observed for the absorption maximum in the DMA dispersion compared to the DCB dispersion, indicating a slight solvatochromic shift based on a difference in the electronic interactions between SWNTs and these two solvents. DCB and DMA show similar dispersion limits (D_L) of $6.25 \leq D_L < 12.5$ μg/mL for our raw SWNT soot, as compared to the previously reported value of 95 μg/mL. This may be attributed to differences in the SWNT materials used, as well as the limited data set in the previous report, which may artificially inflate the dispersion limit values due to a contribution from non-SWNT carbon.[13] Differences in the diameter distribution averages (that for HiPco is 1.0 nm, which is less than that for the laser, 1.37 nm) are well-known,[10] but physical properties such as bundling, defect density, and purity are more difficult to establish. The fact that both DCB and DMA show the ability to form stable SWNT dispersions indicates that a set of structural and electronic properties exists for these solvents, which are capable of interacting favorably with the SWNTs. A recent report has shown that sonochemical polymerization of DCB enhances the dispersing ability of this solvent, but that this effect is not present with DMF solutions.[28] Similarly, we have evaluated DMA before and after ultrasonication and have observed no change in the infrared spectrum even after an exposure time of 4 h. Therefore, the sonochemical polymerizations previously observed with DCB are not suggested to be responsible for the stabilization of SWNTs in alkyl amide solvents.

Evaluation of the Beer's law plots for the absorption maxima of the raw SWNT−alkyl amide solvent dispersions has enabled the determination of extinction coefficients. The values listed in Table 1 display a general trend for both semiconducting (1.27 eV) and metallic (1.77 eV) transitions, i.e., DMP > DEA ≈ DMA > DMF. This trend parallels the electron-donating character of the alkyl groups attached to the carbonyl of the amide. In addition, when the results for DEA and DMA are compared, the alkyl group present on the nitrogen shows a smaller, but consistent, increase in the extinction coefficient. As is common with alkenes, the substituents on the solvents will thermodynamically stabilize the double bond character in the resonance-stabilized amide, which leads to stabilization of the electronic dipole moment in the solvents, and in turn influences the interaction with an SWNT. This explanation is supported by the data, which show a 10−15% increase in the extinction coefficient for DMP compared to DMF. Such a

TABLE 2: MOPAC AM1 Theoretical Calculations for the Bond Lengths and Bond Angles of Alkyl Amide Solvents[a]

solvent	C═O bond length (Å)	C−N bond length (Å)	R−C═O bond angle (deg)	N−C═O bond angle (deg)
DMF	1.242	1.380	122.678	122.909
	(1.224)[32]	(1.391)[32]	(119.5)[32]	(123.5)[32]
DMA	1.249	1.388	120.260	119.979
	(1.226)[33]	(1.368)[33]	(123.1)[33]	(121.0)[33]
DEA	1.248	1.392	120.245	120.419
DMP	1.247	1.391	121.762	120.164

[a] Experimental values from gas electron diffraction (GED) studies are listed in parentheses with appropriate references.

change is significant, since the difference in the index of refraction for DMP ($\eta^{20}_{DMP} = 1.440$) and DMF ($\eta^{20}_{DMF} = 1.431$) would not account for the absorbance increases. The apparent solvent interaction appears to increase the probability of electronic transitions in the SWNTs, resulting in the larger extinction coefficients, although no apparent solvatochromic shift is observed among the four alkyl amide solvents for dispersions of raw soot. The importance of electron donor character toward stabilizing SWNTs in solution has been cited for DMF.[11] However, the current alkyl amide solvents (DMA, DEA, and DMP) have even greater electron-donating ability, leading to higher dispersion capability than observed in DMF. The polarity of these solvents, evident by the dielectric constants (see Table 1), may be an important consideration, since the resulting electronic interaction is largely influenced by changes in the van der Waals forces of the SWNTs with the solvent molecules. However, similar attempts at dispersing SWNTs using acetonitrile (dielectric constant 36.00) and DMSO (dielectric constant 46.71)[29] have been unsuccessful, indicating that dispersion capability is not merely a function of polarity. In addition to the dipole−dipole effects, the interaction between alkyl amide solvents and SWNTs may result from increased π orbital overlap or "stacking",[30] which is greatest for optimized solvent geometries. For example, the π orbital interaction would be significantly higher for 1,2-dichlorobenzene compared to alkyl amide solvents, but the reduced polarity (dielectric constant 10.36)[29] may account for the equivalent dispersion performance. Therefore, in the case of alkyl amide solvents, the presence of a highly polar π system in conjunction with appropriate bond lengths and bond angles should show the highest SWNT dispersion limit.

To maximize the electronic effects between the alkyl amide solvents and SWNTs, a complementary set of steric properties may be necessary. We have performed AM1 theoretical calculations using Chem 3D MOPAC, a general-purpose semiempirical quantum mechanics package, to determine the geometries associated with the alkyl amide solvents.[31] Table 2 lists the calculated bond lengths and bond angles associated with the amide linkage. In addition, experimental values from gas electron diffraction (GED) are provided for corroboration of the theoretical results for DMF and DMA.[32,33] The overall values show good agreement with the structural characteristics described previously for SWNTs.[21] The calculated carbon−carbon bond length in an SWNT is 1.42 Å, while the bond angle is 120°. These results are suggestive of a potential π orbital stacking between the solvent and SWNTs, which is expected to be sensitive to these geometries. The alkyl amide solvent which exhibits the most favorable structural alignment to the carbon−carbon bonding in an SWNT is DMA. Therefore, we propose that the highest SWNT dispersion limit observed in DMA is a result of the highly polar π system, which structurally contains an optimal geometry for interaction with the SWNT backbone. Future work aimed at theoretically modeling this type of interaction, similar to the recent report on DCB, may lend credence to this mechanism.[34]

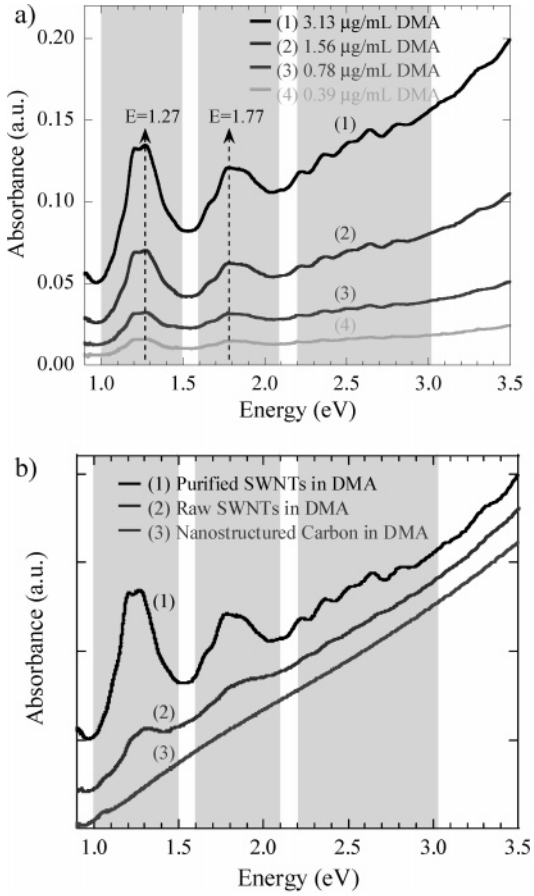

Figure 5. (a) Optical absorption spectra of purified SWNT−DMA dispersions for the series of concentrations used to generate the Beer's law analysis. (b) Optical absorption spectra comparing the relative absorbance intensity of (1) purified SWNTs, (2) raw SWNT soot, and (3) nanostructured carbon in DMA. The spectra, offset for clarity, were all obtained from a 3.13 μg/mL concentration. The gray bands in (a) and (b) depict the energy transition range for the current SWNT diameter distribution.

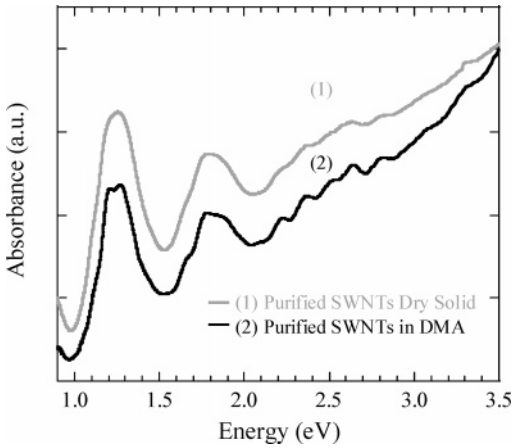

Figure 6. Optical absorption spectra for (1) purified SWNTs sprayed on quartz from acetone solution (gray) and (2) purified SWNTs in DMA (black). Improvement in the peak resolution is distinctly observed for the DMA dispersion compared to the dry solid.

Following the same protocol which was used with raw soot, purified SWNTs were dispersed in DMA, and the corresponding optical absorption spectra were obtained. Selection of DMA was

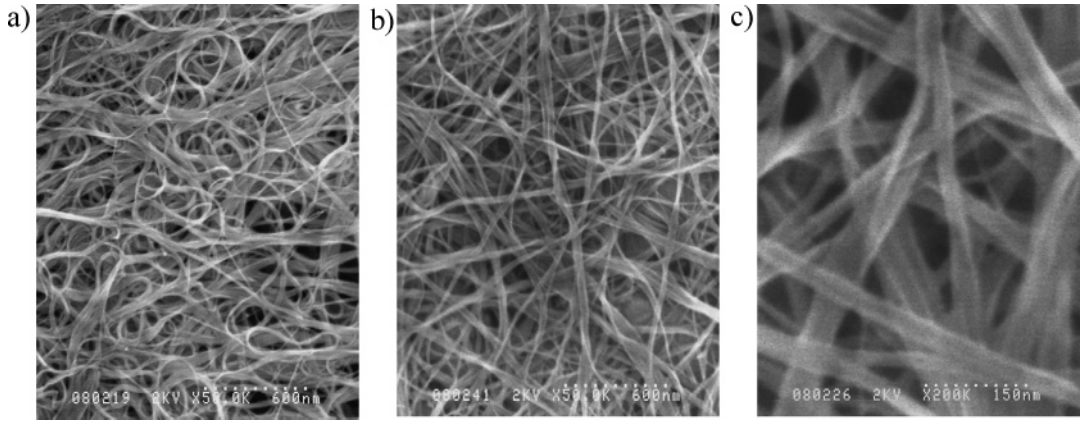

Figure 7. SEM analysis at a magnification of 50000× for purified SWNTs (a) before and (b) after dispersion in DMA. (c) is a high-magnification image of (b) at a magnification of 200000×.

TABLE 3: Experimental Results for Dispersion Limit (D_L) Estimations and Extinction Coefficients of Raw, Purified, and NC Materials Dispersed in DMA

solute	D_L (μg/mL)	$\epsilon_{1.27eV}$ (mL·mg^{-1}·cm^{-1})	$\epsilon_{1.77eV}$ (mL·mg^{-1}·cm^{-1})
raw	6.25	23.8	31.2
purified	3.13	43.4	39.0
NC	325	15.7	25.2

based upon it having the highest observed dispersion limit for the raw SWNT soot. Shown in Figure 5a is an overlay of the spectra used for Beer's law analysis to calculate the estimated dispersion limit and extinction coefficients. The purified SWNT dispersion limit was determined to be 3.13 μg/mL in DMA, on the basis of the described method. The presence of carboxylic acid groups from the nitric acid processing[9] on the purified SWNTs may influence the dispersion in DMA; however, purified−annealed SWNTs showed similar dispersion limits. The extinction coefficients for purified SWNTs in DMA were calculated to be 43.4 and 39.0 mL·mg^{-1}·cm^{-1} at 1.27 and 1.77 eV, respectively. Summarized in Table 3 are the dispersion limit and extinction coefficient results comparing the purified SWNTs with raw SWNT soot and nanostructured carbon. The characteristic differences in absorption properties for each of these carbon-based materials can be observed in the spectral overlay shown in Figure 5b. The relationship between absorption intensity and peak resolution for the SWNT transitions can be directly related to the SWNT mass fraction of a sample. The calculated extinction coefficients can be used to estimate the relative SWNT concentration in a laser-generated sample for the established diameter distribution and semiconducting-to-metallic ratio. It is important to recognize that the magnitude of the extinction coefficient is dependent on both the solvent effects (Table 1) and the SWNT sample purity (Table 3). Other potential SWNT physical properties that may influence the extinction coefficients include diameter, length, and bundling effects. These considerations may account for the variation in extinction coefficients reported thus far for SWNTs.[13,14]

An important advantage of SWNT−solvent dispersions over other dispersing strategies is the ability to easily remove the solvent through evaporation and recover the starting material. The optical absorption overlay shown in Figure 6 depicts the differences in purified SWNTs air sprayed from acetone onto a quartz slide (dry solid) and purified SWNTs dispersed in DMA. The enhanced resolution of the SWNT transitions for the DMA dispersion may be attributed to a debundling effect, in analogy with optical absorption spectra of surfactant-stabilized SWNTs. This implies that smaller bundles or individual SWNTs are present in the DMA dispersion.[6] Additionally, SEM images were obtained from SWNTs that were forced to aggregate into bundles from a DMA dispersion by solvent evaporation, prior to analysis. The results for purified SWNTs before and after dispersion in DMA indicate the presence of bundles for both cases, albeit the precipitated SWNTs appear to have a more straightened, "relaxed" structure (Figure 7). Therefore, the dispersion process appears to suspend the SWNTs without apparent damage to the underlying structure, although future analysis of any chemical functionalization is warranted. The dispersion results described here are not unique to purified laser-generated SWNTs; similar dispersion behavior in DMA using purified HiPco[35] has also been demonstrated.

Conclusion

The capability for a series of alkyl amide solvents to disperse as-produced raw and purified SWNTs has been evaluated. Characterization using optical absorption spectroscopy has enabled calculation of the dispersion limit and extinction coefficients for the laser-generated semiconducting and metallic SWNTs. The highly polar π system and optimal geometries of the alkyl amide solvents are proposed to be the factors responsible for the dispersion of SWNTs. The best dispersion of the solvents studied was in DMA, which also corresponded to the best combination of steric and electronic factors. These SWNT−DMA dispersions proved to be stable for days to even weeks. The optical absorption spectra generated from these dispersions showed well-resolved fine structure, presumably due to debundling. Production of stable SWNT dispersions without the use of any external agent (i.e., surfactant, polymer, amine, etc.) emerges as a powerful strategy toward probing the properties of SWNTs. Specifically, the extinction coefficients for purified SWNTs can be used to monitor the relative SWNT mass fraction during the purification process. Ultimately, the use of SWNT−solvent dispersions in electrophoretic separations may lead to phase-pure SWNTs on the basis of diameter and type.

Acknowledgment. We thank Thomas Gennett, Jeffrey M. Elich, and William VanDerveer for their help in the development of our SWNT synthesis and purification capabilities and Eileen Baumgartner for her photographic assistance. Financial support for this project was from the National Science Foundation (Grant No. ECS-0233776), the Department of Energy (Grant No. DE-FG02-02ER63393), NASA (Grant Nos. NAG3-2828 and NCC3-956), and the Rochester Institute of Technology's First In Class Initiative.

Supporting Information Available: Raman spectra of the RBM for laser-generated SWNTs (PDF). This material is available free of charge via the Internet at http://pubs.acs.org.

References and Notes

(1) Dai, H. *Surf. Sci.* **2002**, *500*, 218.

(2) Peng, H.; Alemany, L. B.; Margrave, J. L.; Khabashesku, V. N. *J. Am. Chem. Soc.* **2003**, *125*, 15174.

(3) Kahn, M. G. C.; Banerjee, S.; Wong, S. S. *Nano Lett.* **2002**, *2*, 1215.

(4) Landi, B. J.; Raffaelle, R. P.; Heben, M. J.; Alleman, J. L.; VanDerveer, W.; Gennett, T. *Nano Lett.* **2002**, *2* (11), 1329.

(5) O'Connell, M. J.; Boul, P.; Ericson, L. M.; Huffman, C.; Wang, Y.; Haroz, E.; Kuper, C.; Tour, J.; Ausman, K. D.; Smalley, R. E. *Chem. Phys. Lett.* **2001**, *342*, 265−271.

(6) O'Connell, M. J.; Bachilo, S. M.; Huffman, C. B.; Moore, V. C.; Strano, M. S.; Haroz, E. H.; Rialon, K. L.; Boul, P. J.; Noon, W. H.; Kittrell, C.; Ma, J.; Hauge, R. H.; Weisman, R. B.; Smalley, R. E. *Science* **2002**, *297*, 593.

(7) Matarredona, O.; Rhoads, H.; Li, Z.; Harwell, J. H.; Balzano, L.; Resasco, D. E. *J. Phys. Chem. B* **2003**, *107*, 13357.

(8) Chen, J.; Hamon, M. A.; Hu, H.; Chen, Y.; Rao, A. M.; Eklund, P. C.; Haddon, R. C. *Science* **1998**, *282*, 95.

(9) Chen, J.; Rao, A. M.; Lyuksyutov, S.; Itkis, M. E.; Hamon, M. A.; Hu, H.; Cohn, R. W.; Eklund, P. C.; Colbert, D. T.; Smalley, R. E.; Haddon, R. C. *J. Phys. Chem. B* **2001**, *105*, 2525.

(10) Chattopadhyay, D.; Galeska, I.; Papadimitrakopoulos, F. *J. Am. Chem. Soc.* **2003**, *125*, 3370.

(11) Ausman, K. D.; Piner, R.; Lourie, O.; Ruoff, R. S.; Korobov, M. *J. Phys. Chem. B* **2000**, *104* (38), 8911.

(12) Krupke, R.; Hennrich, F.; Hampe, O.; Kappes, M. M. *J. Phys. Chem. B* **2003**, *107*, 5667.

(13) Bahr, J. L.; Mickelson, E. T.; Bronikowski, M. J.; Smalley, R. E.; Tour, J. M. *Chem. Commun.* **2001**, *2*, 193.

(14) Zhou, B.; Lin, Y.; Li, H.; Huang, W.; Connell, J. W.; Allard, L. F.; Sun, Y. P. *J. Phys. Chem. B* **2003**, *107*, 13588.

(15) Gennett, T.; Dillon, A. C.; Alleman, J. L.; Jones, K. M.; Parilla, P. A.; Heben, M. J. *Mater. Res. Soc. Symp. Proc.* **2001**, *633*, A9.1.1−A9.1.11.

(16) Kataura, H.; Kumazawa, Y.; Maniwa, Y.; Umezu, I.; Suzuki, S.; Ohtsuka, Y.; Achiba, Y. *Synth. Met.* **1999**, *103*, 2555.

(17) Dillon, A. C.; Gennett, T.; Jones, K. M.; Alleman, J. L.; Parilla, P. A.; Heben, M. J. *Adv. Mater.* **1999**, *11* (16), 1354−1358.

(18) Martinez, M. T.; Callejas, M. A.; Benito, A. M.; Cochet, M.; Seeger, T.; Anson, A.; Schreiber, J.; Gordon, C.; Marhic, C.; Chauvet, O.; Fierro, J. L. G.; Maser, W. K. *Carbon* **2003**, *41*, 2247.

(19) Lian, Y.; Maeda, Y.; Wakahara, T.; Akasaka, T.; Kazaoui, S.; Minami, N.; Choi, N.; Tokumoto, H. *J. Phys. Chem. B* **2003**, *107*, 12082.

(20) Odom, T. W.; Huang, J.-L.; Kim, P.; Lieber, C. M. *Nature* **1998**, *391*, 62.

(21) Wildoer, J. W. G.; Venema, L. C.; Rinzler, A. G.; Smalley, R. E.; Dekker, C. *Nature* **1998**, *391*, 59.

(22) Hagen, A.; Hertel, T. *Nano Lett.* **2003**, *3* (3), 383.

(23) Itkis, M. E.; Perea, D. E.; Niyogi, S.; Rickard, S. M.; Hamon, M. A.; Hu, H.; Zhao, B.; Haddon, R. C. *Nano Lett.* **2003**, *3*, 309.

(24) Dresselhaus, M. S.; Dresselhaus, G.; Jorio, A.; Souza Filho, A. G.; Saito, R. *Carbon* **2002**, *40*, 2043.

(25) Rao, A. M.; Chen, J.; Richter, E.; Schlecht, U.; Eklund, P. C.; Haddon, R. C.; Venkateswaran, U. D.; Kwon, Y.-K.; Tomanek, D. *Phys. Rev. Lett.* **2001**, *86* (17), 3895−3898.

(26) Strong, F. C. *Anal. Chem.* **1952**, *24*, 338.

(27) Skoog, D. A.; Holler, F. J.; Nieman, T. A. In *Principles of Instrumental Analysis*, 5th ed.; Harcourt Brace & Co.: Philadelphia, 1998; p 303.

(28) Niyogi, S.; Hamon, M. A.; Perea, D. E.; Kang, C. B.; Zhao, B.; Pal, S. K.; Wyant, A. E.; Itkis, M. E.; Haddon, R. C. *J. Phys. Chem. B* **2003**, *107*, 8799.

(29) Laurence, C.; Nicolet, P.; Dalati, M. T.; Abboud, J. L. M.; Notario, R. *J. Phys. Chem. B* **1994**, *98*, 5807.

(30) Chen, R. J.; Zhang, Y.; Wang, D.; Dai, H. *J. Am. Chem. Soc.* **2001**, *123*, 3838.

(31) Arora, K. *Asian J. Chem.* **2002**, *14*, 1719.

(32) Schultz, G.; Hargittai, I. *J. Phys. Chem.* **1993**, *97*, 4966.

(33) Mack, H. G.; Oberhammer, H. *J. Am. Chem. Soc.* **1997**, *119*, 3567.

(34) Fagan, S. B.; Souza Filho, A. G.; Lima, J. O. G.; Mendes Filho, J.; Ferreira, O. P.; Mazali, I. O.; Alves, O. L.; Dresselhaus, M. S. *Nano Lett.* **2004**, *4* (7), 1285−1288.

(35) Chiang, I. W.; Brinson, B. E.; Huang, A. Y.; Willis, P. A.; Bronikowski, M. J.; Margrave, J. L.; Smalley, R. E.; Hauge, R. H. *J. Phys. Chem. B* **2001**, *105*, 8297.